Original Article | Experimental and Others

http://dx.doi.org/10.3348/kjr.2014.15.2.195
pISSN 1229-6929 · eISSN 2005-8330
Korean J Radiol 2014;15(2):195-204

Korean Journal of Radiology
KJR

Adaptive Iterative Dose Reduction Algorithm in CT: Effect on Image Quality Compared with Filtered Back Projection in Body Phantoms of Different Sizes

Milim Kim[1], Jeong Min Lee, MD, PhD[2, 3], Jeong Hee Yoon, MD[2], Hyoshin Son[1], Jin Woo Choi, MD[2], Joon Koo Han, MD[2, 3], Byung Ihn Choi, MD[2, 3]

[1]College of Medicine, Seoul National University, Seoul 110-744, Korea; [2]Department of Radiology, Seoul National University Hospital, Seoul 110-744, Korea; [3]Research Institute of Radiation Medicine, Seoul National University College of Medicine, Seoul 110-744, Korea

Objective: To evaluate the impact of the adaptive iterative dose reduction (AIDR) three-dimensional (3D) algorithm in CT on noise reduction and the image quality compared to the filtered back projection (FBP) algorithm and to compare the effectiveness of AIDR 3D on noise reduction according to the body habitus using phantoms with different sizes.

Materials and Methods: Three different-sized phantoms with diameters of 24 cm, 30 cm, and 40 cm were built up using the American College of Radiology CT accreditation phantom and layers of pork belly fat. Each phantom was scanned eight times using different mAs. Images were reconstructed using the FBP and three different strengths of the AIDR 3D. The image noise, the contrast-to-noise ratio (CNR) and the signal-to-noise ratio (SNR) of the phantom were assessed. Two radiologists assessed the image quality of the 4 image sets in consensus. The effectiveness of AIDR 3D on noise reduction compared with FBP were also compared according to the phantom sizes.

Results: Adaptive iterative dose reduction 3D significantly reduced the image noise compared with FBP and enhanced the SNR and CNR ($p < 0.05$) with improved image quality ($p < 0.05$). When a stronger reconstruction algorithm was used, greater increase of SNR and CNR as well as noise reduction was achieved ($p < 0.05$). The noise reduction effect of AIDR 3D was significantly greater in the 40-cm phantom than in the 24-cm or 30-cm phantoms ($p < 0.05$).

Conclusion: The AIDR 3D algorithm is effective to reduce the image noise as well as to improve the image-quality parameters compared by FBP algorithm, and its effectiveness may increase as the phantom size increases.

Index terms: *Adaptive iterative dose reduction; CT, phantom study; Body sizes*

INTRODUCTION

The recent development of multidetector CT (MDCT) has caused an explosive growth in the number of CT examinations. This can be attributed to its wide availability, speed and diagnostic benefits (1, 2). Although the widespread use of MDCT examinations for the evaluation of various abdominal diseases may result in significant improved diagnostic performances, there has been considerable concern regarding the increased radiation exposure and the risk of radiation-induced cancer (3-5). In order to address the concerns regarding the radiation dose associated with CT, several approaches have been used to reduce the radiation dose, including automated tube current modulation, dynamically adjustable z-axis X-ray beam collimation and the use of a volumetric acquisition mode to reduce the over-ranging phenomenon (6-14).

Received December 11, 2012; accepted after revision January 14, 2014.
This study was supported by 2012 Man Chung Han Research Grant.
Corresponding author: Jeong Min Lee, MD, PhD, Department of Radiology and Research Institute of Radiation Medicine, Seoul National University College of Medicine, 101 Daehak-ro, Jongno-gu, Seoul 110-744, Korea.
• Tel: (822) 760-3154 • Fax: (822) 743-6385
• E-mail: jmsh@snu.ac.kr

However, despite the development of dose reduction technologies, dose reduction remains limited if filtered back projection (FBP) reconstructions are used (15). Indeed, FBP reconstructions create a significant increase in image noise when the dose is reduced excessively (16). More recently, several iterative reconstruction (IR) techniques, including ASIR™, Veo™ (GE Healthcare, Waukesha, WI, USA), iDose™, iDose4™ (Philips Healthcare, Cleveland, OH, USA), and IRIS™ and SAFIRE™ (Siemens Healthcare, Forchheim, Germany) have been introduced with the attempt to solve this problem (17-19) and several studies demonstrated that IR techniques can achieve a significant dose reduction up to 66% compared with FBP reconstructions (6, 12, 15, 20). However, some researchers have encountered image quality problems such as artificial texture or a blotchy appearance when high strength of IR is used. And profound changes in the image appearance with higher levels of iterative weighing could adversely affect the diagnostic confidence level (15, 21). Furthermore, this problem seemed to be more serious when a lower dose was used for patients with larger body size (22).

Recently, a three-dimensional (3D), adaptive iterative dose reduction (AIDR) algorithm (Toshiba Medical Systems Corporation, Otawara, Japan) which concerns raw-data-based, statistical IR techniques and consists of a dual-model, i.e., noise and anatomical technique, has been developed and can be applied to volumetric and wide-volume modes (20). AIDR 3D is the manufacturer's commercial hybrid IR algorithm which combines reconstruction and noise reduction in the raw data and image space domain. The adaptation of AIDR 3D to the diversities of various patients, the scanning parameters and the scanner itself is explicitly implemented using the statistical models of noise and the scanner model in to operate the projection data and by adapting the filter strength according to the relative noise level. In addition, in the image space, AIDR 3D uses a special algorithm of adaptive, weighted, anisotropic diffusion for de-noising with edge preservation in order to reduce noise while maintaining edge structures and noise texture. For the final new feature of AIDR 3D can be said to be that it is blending of the image initially reconstructed using the FBP algorithm and the image resulting from the iterative processing in the image space. The intention is to maintain the natural appearances of FBP which is already familiar to radiologists. In AIDR 3D processing, a statistical noise model considering both the photon and electronic noise, is used to eliminate noise caused by photon starvation in the projection data. Furthermore, the AIDR 3D technique has been designed to be fully integrated into the Automatic Exposure Control (SUREExposure, Toshiba Medical Systems Corporation, Otawara, Japan) (14). Therefore, theoretically, this technique can choose the amount of dose reduction (50–75%) for CT scanning, regardless of the patient's body size and also can choose a different strength of IR as to improve the spatial resolution. However, there has been no definite proof whether the AIDR 3D technique can effectively reduce image noise even in large body habitus patients, similar to that which occurs in small body habitus patients until now.

Therefore, the purpose of this study was to evaluate the impact of the AIDR 3D algorithm on noise reduction and the image quality compared to that of the FBP algorithm and to compare the effectiveness of AIDR 3D on noise reduction according to the body habitus using phantoms of different sizes.

MATERIALS AND METHODS

This phantom study was conducted to evaluate the impact of the AIDR 3D algorithm on the image quality compared to that of the FBP algorithm in phantoms mimicking different patient body sizes (20) and also to determine whether different strengths of AIDR can equally reduce the tube current in different-sized phantoms.

Phantoms

The American College of Radiology (ACR) CT Accreditation Phantom (Gammex 464; Gammex Inc., Middleton, WI, USA), was used to create phantoms with varying sizes. It was originally designed for the ACR CT accreditation program. The phantom size was 20 cm in diameter and 16 cm long. The matrix material was solid water with 0 ± 5 Hounsfield units (HU). The phantom was composed of four modules and the first module was used in this study. The imbedded test objects in module 1 were a water-equivalent linearity rod (0 HU), bone equivalent linearity rod (955 HU), air (-1000 HU), acrylic linearity rod (120 HU), and a polyethylene linearity rod (-95 HU).

In order to mimic the different body sizes of humans, we produced three phantoms of different sizes, i.e., 24 cm in diameter, 30 cm in diameter, and 40 cm in diameter by covering the ACR CT Accreditation Phantom with one to three layers of pork belly fat (Fig. 1). The smallest phantom

Korean Journal of Radiology
KJR

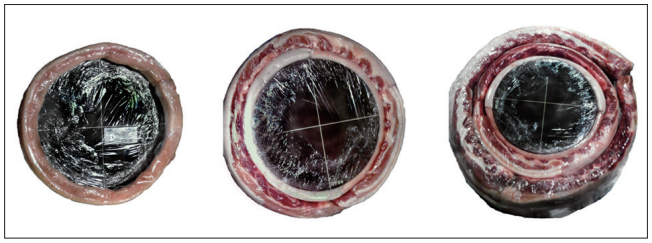

Fig. 1. Images of three phantoms with different thicknesses of subcutaneous fat: 24-cm-diameter phantom (left); 30-cm-diameter phantom (middle); and 40-cm-diameter phantom (right).

(24 cm in diameter) was made by directly covering the phantom with one layer of pork belly fat (2-cm thickness), thus mimicking a person with a waist circumference of 29.6 inches. The medium-sized phantom (30 cm in diameter) mimicked an approximately 37-inch-waist size person and the largest phantom (40 cm in diameter) mimicked an approximately 49.4-inch-waist size person. The latter both were made by covering the ACR CT phantom with two layers of pork belly fat of 5-cm thickness and with three layers of pork belly fat of 10-cm thickness. All three layers were covered with plastic wrap and were taped to the ACR CT phantom.

CT Acquisition

CT scanning was performed on a 320-detector-row CT scanner (Aquillion ONE; Toshiba Medical Systems Corporation, Tokyo, Japan). The protocol consisted of acquisition of a CT volume data covering the entire phantom with eight different tube current values, i.e., 100, 120, 140, 160, 180, 200, 250, and 290 mAs for all three phantom models. The detailed CT parameters were as follows: tube energy 120 kVp; collimation 80 x 0.5 mm; rotation time 0.5 seconds; and pitch 0.75. The computed tomography dose index (CTDI) and the dose length product (DLP) were recorded for each mAs. An automatic tube current modulation software (^{Sure}Exposure 3D, Toshiba Medical Systems Corporation, Otawara, Japan) was not used as it can produce minor changes in the tube current-time product settings in each scan. Instead, eight fixed-tube, current-time product settings were used as they can deliver exactly the same image noise as predicted. Other benefits of the use of a fixed tube current technique could include better comparability and reproducibility with CT scanners from other manufacturers. The phantom was positioned within the isocenter of the CT scanner with its cross-section perpendicular to the scanner's z-axis.

Image Reconstruction

Then 4 different types of images were reconstructed for each scan using the traditional 3D FBP technique as well as the hybrid IR algorithm (AIDR 3D, Toshiba Medical Systems Corporation) using 3 different strengths, i.e., mild, standard or strong level. Therefore, 32 image sets were reconstructed for 3 different-sized phantoms and a total of 96 reconstructed image sets were obtained. The FBP and AIDR 3D data sets were reconstructed with the same reconstruction filter FC 04.

Image Quality Evaluation

All images were analyzed on a Picture Archiving and Communication System (PACS) (Maroview 5.4, Infinitt, Seoul, Korea) using monitors with a spatial resolution of 1600 x 1200 (Totoku Electric Co., Ltd, Kanagawa, Japan).

Quantitative Analysis

The image quality was quantitatively evaluated by measuring image noise, the signal-to-noise ratio (SNR), and the contrast-to-noise ratio (CNR). One reader drew the circular region of interests (ROIs) on module 1. To ensure consistency, all measurements were performed three times and the mean values were calculated. Module 1 of the phantom was built up for the evaluation of 5 different materials, i.e., polyethylene, bone, air, water and acryl. A total of 3 circular ROIs (2.0 ± 0.5 cm^2) were drawn at the center of the different phantom composites, i.e., on the acryl (ROI #1), on the water portion in the center of the phantom (ROI #2) and in the background area adjacent to the measured target (ROI #3). All 3 ROIs were measured on the slice with a clearly shown alignment line of the module 1 phantom.

As the noise corresponded to the measurement of the standard deviation (SD) of the measured HU of ROI #1, the acrylic phantom data was selected for assessing the SNR and the CNR as it may mimic attenuation features of soft tissue (20). The ratio between the mean attenuation value of ROI #1 (acrylic phantom) and the SD of ROI #1 corresponded to the SNR, which can be expressed as a equation: ROI_m/SD_m, where ROI_m is the CT number of the acrylic phantom and SD_m is the SD of the acrylic phantom (23). Whereas the difference ratio in the mean attenuation of the two ROIs (ROI #1 and ROI #2) and the SD of ROI #2 (noise) corresponded to the CNR, which is calculated as follows: $(ROI_m - ROI_B) / SD_B$, where ROI_m and ROI_B are the numbers of CT measured in the acrylic phantom and the background ROI and SD is

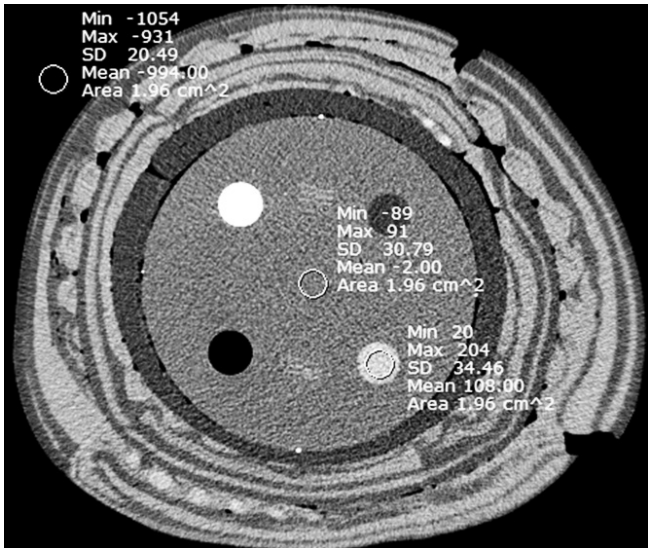

Fig. 2. Region of interest circles drawn for quantitative analysis of phantom study on CT image of 40-cm phantom reconstructed with filtered back projection at tube current time product of 200 mAs.

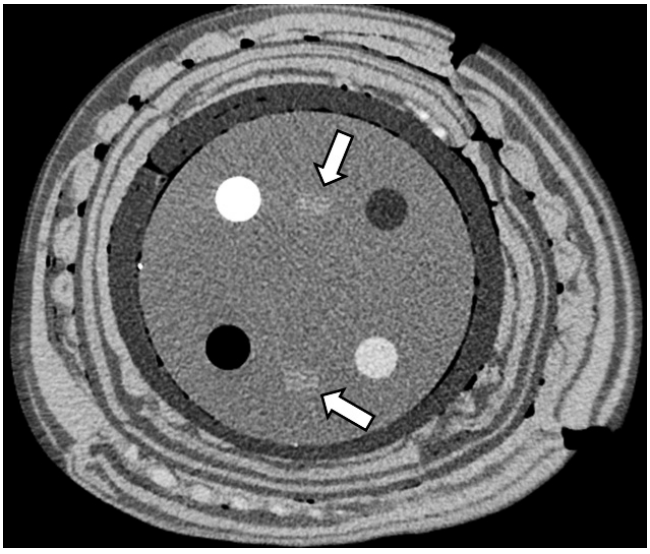

Fig. 3. CT image of module 1 of 40-cm phantom reconstructed with adaptive iterative dose reduction three-dimensional standard mode at tube current time product of 180 mAs, showing alignment line (arrows).

the SD of the background (Fig. 2) (24).

Qualitative Analysis

Under consideration of artifacts and using a five point scale, two blinded radiologists with 22 years respectively 3 years of clinical experience in radiology jointly assessed in consensus the 96 image sets regarding image noise, lesion conspicuity and overall image quality. All CT images were reviewed on a PACS. Prior to the evaluation process, the two radiologists agreed in consensus regarding the evaluation criteria using a 5-point scale and with standard reference images for each grade. The representative images, scanned through module 1 of the ACR accreditation phantom and showing all 5 internal markers as well as the alignment markers, were selected for qualitative analysis (Fig. 3).

The overall image quality was graded using a 5-point scale in which a score of 5 indicated excellent; a score of 4, better than average; a score of 3, average; a score of 2, worse than average; and a score of 1, unacceptable diagnostic image quality (25). The image noise was graded according to the presence and amount of mottle or graininess in the images with use of a 5-point scale in which a score of 1 indicated unacceptable noise; a score of 2, above-average increased noise; a score of 3, average noise in an acceptable image; a score of 4, less than average noise; and a score of 5, minimum or no image noise. Lesion conspicuity of the alignment lines in module 1 of the phantom were assessed using a 5-point scale as follows: a score of 1 indicated the definite presence of an artifact that mimicked a lesion; a score of 2, the presence of a suspicious lesion or an artifact that mimicked a lesion; a score of 3, the presence of a subtly noted lesion with ill-defined margins; a score of 4, the presence of a clearly visible lesion with poorly visualized margins; and a score of 5, the presence of a clearly visible lesion with well-visualized margins (26).

Statistical Analysis

In order to demonstrate the effectiveness of the AIDR 3D reconstruction algorithm with 3 different strengths to reduce image noise and improve the SNR and CNR compared to the FBP algorithm, the quantitative image parameters of the 4 image sets were compared for each of the 3 phantoms, using the repeated measures analysis of variance (ANOVA) and the Bonferroni correction. In addition, the relative changes (%) in image noise, SNR and CNR in the AIDR 3D algorithm with 3 different strengths compared to the FBP, were analyzed using the repeated measures ANOVA and Bonferroni correction for each of the 3 phantoms. For these analysis of quantitative parameters, each of the 4 image sets (AIDR 3D mild, standard, strong settings and FBP) of the 3 phantoms had 8 CT data sets, as those CT scans were obtained with 8 different tube current time products (100–290 mAs). A Bonferroni corrected p value < 0.05 was regarded as statistically significant to compare the intergroup. Also a comparison of the qualitative analysis

Korean Journal of Radiology
KJR

results was performed among the 3 AIDR 3D image sets and the FBP image set. First the Friedman test was used and thereafter the Wilcoxon signed rank test to compare the intergroup. A p value < 0.017 was considered as statistical significant.

Secondly, to determine whether the effectiveness of the AIDR 3D algorithm was affected by the phantom size, the percentage of noise reduction of the AIDR 3D standard algorithm was compared with FBP in different-sized phantoms: i.e., 24 cm, 30 cm, and 40 cm in diameters, using ANOVA test with Bonferroni correction. The noise reduction could be expressed as an equation: 1 - ($Noise_b$ / $Noise_a$). $Noise_a$ was the noise value of AIDR 3D, whereas $Noise_b$ was the noise of FBP. For this comparison, the percentage of noise reductions of the AIDR 3D standard algorithm compared with FBP in each of the 3 phantoms was determined for with different tube current time products (100–290 mAs) for 8 CT scans.

All statistical analyses were performed using commercially available software (SPSS, version 17.0; SPSS Inc., Chicago, IL, USA).

RESULTS

The $CTDI_{vol}$ and the DLP (DLP = $CTDI_{vol}$ x scan length) of CT scans at each mAs were in range of 12.2–35.1 mGy and 362.8–1052 mGy·cm, respectively.

Quantitative Analysis

Comparison of AIDR 3D and FBP for Image Noise, SNR and CNR

When the FBP and the 3 AIDR 3D reconstructed CT image sets of the 3 phantom models obtained with 8 different tube current values (100–290 mAs) were compared for noise, SNR and CNR, the noise values of the AIDR 3D reconstructed images, were lower than those of the FBP images regardless of the degree of strength. In addition, also the average CNR and SNR of the AIDR 3D images sets were higher than those of the FBP image sets (p < 0.05) (Table 1).

When AIDR 3D was used, the relative changes in noise, SNR and CNR in percentages, confirm the raw data as well as all of the quantitative parameters improved greatly. And a better SNR, CNR and noise reduction were achieved when a stronger reconstruction algorithm was used (p < 0.05) (Table 2). In particular, in the 24-cm phantom model, an average of 11.7%, 22.6%, and 30.5% image noise reduction was achieved using the mild, standard and strong AIDR 3D techniques, respectively (Table 2).

Impact of Body Habitus on the Effectiveness of AIDR for Image Noise Reduction

Regarding the degree of image noise reduction, the AIDR 3D technique was even more effective with the 40-cm phantom than with 24-cm and 30-cm phantoms (Table 3). The percentage of noise reduction of AIDR 3D was also

Table 1. Noise, SNR, and CNR from Phantom Imaging in Different-Sized Phantoms

Phantom Size	Reconstruction Method	24 cm			30 cm			40 cm		
		Average	P*	$P_{1,2,3}$†	Average	P*	$P_{1,2,3}$†	Average	P*	$P_{1,2,3}$†
Noise	FBP	9.63	0.001	< 0.05	16.53	0.002	< 0.05	30.69	0.001	< 0.05
	Mild	8.46			12.025			20.78		
	STD	7.41			10.575			17.74		
	STR	6.66			9.368			15.20		
SNR	FBP	13.45	0.011	< 0.05	7.49	0.013	< 0.05	3.10	0.001	< 0.05
	Mild	15.22			10.23			5.40		
	STD	17.37			11.61			6.35		
	STR	19.33			13.10			7.41		
CNR	FBP	12.17	0.001	< 0.05	7.80	0.001	< 0.05	3.52	0.001	< 0.05
	Mild	13.85			9.84			5.93		
	STD	15.80			11.40			6.94		
	STR	17.62			12.68			7.63		

Note.— Average values for all data using 100, 120, 140, 160, 180, 200, 250, and 290 mAs, respectively, are shown. *P value indicates p value from repeated measures analysis of variance, †$P_{1,2,3}$ indicates that all three p values from Bonferroni correction are < 0.05. AIDR = adaptive iterative dose reduction, CNR = contrast-to-noise ratio, FBP = filtered back projection, Mild = AIDR mild reconstruction algorithm, SNR = signal-to-noise ratio, STD = AIDR standard reconstruction algorithm, STR = AIDR strong reconstruction algorithm, 24 = 24-cm phantom, 30 = 30-cm phantom, 40 = 40-cm phantom, respectively

Table 2. Effectiveness of AIDR 3D Algorithm with Three Different Strengths for Image Noise Reduction and Improvement of SNR and CNR in Different-Sized Phantom Models

		Relative Changes in Noise, SNR, and CNR with AIDR Techniques Compared with FBP			*P*	P_1 & P_2
		Mild	STD	STR		
Noise	24 cm	-11.66	-22.60	-30.51	0.001	0.001
	30 cm	-27.18	-35.85	-43.19	0.001	0.001
	40 cm	-42.95	-51.32	-58.20	0.001	0.001
SNR	24 cm	13.56	29.60	44.22	0.001	0.001
	30 cm	36.86	55.47	75.37	0.001	0.001
	40 cm	75.47	106.08	140.95	0.001	0.001
CNR	24 cm	13.58	29.81	44.97	0.001	0.001
	30 cm	31.01	51.74	68.83	0.001	0.001
	40 cm	70.47	99.32	113.87	0.001	$P_1 < 0.001$, $P_2 < 0.05$

Note.— Average values for all data using 100, 120, 140, 160, 180, 200, 250, and 290 mAs, respectively, are shown. Values indicate percentage of relative decrease or increase of noise, SNR or CNR after applying different strengths of AIDR techniques: negative values indicate decrease of value in percentage, whereas positive values indicate increase of value in percentage. P_1 indicates difference in noise reduction between Mild and Standard settings compared with FBP, and P_2 indicates difference in noise reduction between Standard and Strong setting compared with FBP. AIDR = adaptive iterative dose reduction, CNR = contrast-to-noise ratio, FBP = filtered back projection, Mild = mild reconstruction algorithm, SNR = signal-to-noise ratio, STD = standard reconstruction algorithm, STR = strong reconstruction algorithm, 3D = three-dimensional

Table 3. Comparison of Effectiveness of AIDR 3D Standard Setting on Noise Reduction Depending on Phantom Size

Tube Current-Time Product (TCTP, mAs)	CTDI	DLP	Noise Level						% of Noise Reduction with AIDR 3D Standard			
			FBP			AIDR Standard						
			24 cm	30 cm	40 cm	24 cm	30 cm	40 cm	24 cm	30 cm	40 cm	*P**, $P_{1,2,3}$†
100	12.2	362.8	12.71	20.73	51.22	9.09	13.78	21.57	28.48	33.53	57.89	
120	14.6	435.3	11.55	19.51	39.88	9.07	12.41	21.29	21.47	36.39	46.61	
140	17.1	507.9	10.98	18.79	38.90	8.32	10.84	19.56	24.23	42.31	49.72	
160	19.5	580.4	9.54	16.71	38.32	7.05	10.42	18.36	26.10	37.64	52.09	
180	21.9	653.0	8.80	15.72	37.48	6.95	10.36	17.62	21.02	34.10	52.99	
200	24.4	725.5	8.09	14.61	31.55	6.68	9.99	15.88	17.43	31.62	49.67	
250	30.5	906.9	8.01	14.02	28.20	6.64	8.47	14.23	17.10	39.59	49.54	
290	35.1	1052.0	7.33	12.18	27.99	5.50	8.33	13.43	24.97	31.61	52.02	
Average			9.63	16.53	36.69	7.41	10.58	17.74	22.60	35.85	51.32	< 0.001, $P_{1,2,3} < 0.001$

Note.— **P* value indicates differences in % of noise reduction after using AIDR standard setting compared with FBP, depending on size of phantoms by repeated measures analysis of variance test, †P_1, P_2, and P_3 indicates *p* values from Bonferroni correction: P_1 represents difference in % of noise reduction with AIDR standard setting between 24 cm and 30cm phantom; P_2 represents difference in % of noise reduction with AIDR standard setting between 24-cm and 40-cm phantom; and P_3 represents difference in % of noise reduction with AIDR standard setting between 30-cm and 40-cm phantom, respectively. AIDR = adaptive iterative dose reduction, CTDI = computed tomography dose index, DLP = dose length product, FBP = filtered back projection, TCTP = tube current-time product, 3D = three-dimensional, 24 cm = 24-cm phantom, 30 cm = 30-cm phantom, 40 cm = 40-cm phantom

greater in 30-cm phantoms than in 24-cm phantoms ($p < 0.05$). The average percentage of noise reduction of the AIDR 3D standard setting compared with FBP in 24-cm, 30-cm, and 40-cm phantoms was 22.6%, 35.9%, and 51.3%, respectively. Compared to the 24-cm phantom model (noise reduction range: 17.1–28.4%), the 30-cm phantom showed even greater noise reduction (range: 31.6–42.3%) when the AIDR 3D algorithm was used, and the 40-cm phantom model showed the most noise reduction (range: 46.6–57.9%) when using the AIDR 3D algorithm, compared to the other phantoms ($p < 0.05$). Regarding the noise reduction, the AIDR 3D reconstruction algorithm was more effective in larger-sized phantoms ($p < 0.05$).

Qualitative Analysis

According to the consensus review by the two radiologists regarding the image noise, lesion conspicuity and the overall image evaluation of all 3 different-sized phantoms

Korean Journal of Radiology
KJR

Table 4. Qualitative Analysis Results of AIDR 3D Image Sets and FBP Image Set in Different-Sized Phantoms

Phantom Size	Analysis Item	Reconstruction Algorithm				P^*, $P_{1,2,3}^{\dagger}$
		FBP	AIDR-Mild	AIDR-STD	AIDR-STR	
24 cm	Image noise	4.13 ± 0.99	4.63 ± 0.52	4.88 ± 0.35	4.88 ± 0.35	0.013, $P_{1,2,3} > 0.017$
	Lesion conspicuity	4.75 ± 0.46	4.88 ± 0.35	4.88 ± 0.35	4.88 ± 0.35	0.392
	Overall image quality	4.13 ± 0.99	4.63 ± 0.52	4.75 ± 0.46	4.75 ± 0.46	0.012, $P_{1,2,3} > 0.017$
30 cm	Image noise	3.00 ± 0.76	4.00 ± 0.76	4.00 ± 0.76	4.50 ± 0.93	0.001, $P_{1,2,3} < 0.017$
	Lesion conspicuity	3.13 ± 0.99	3.75 ± 0.89	3.88 ± 0.83	4.00 ± 0.76	0.001, $P_{2,3} < 0.017$
	Overall image quality	2.50 ± 0.76	3.38 ± 1.19	3.88 ± 1.25	4.00 ± 1.07	0.001, $P_3 < 0.017$
40 cm	Image noise	2.13 ± 0.83	3.25 ± 1.04	3.88 ± 0.83	4.00 ± 0.76	0.001, $P_{1,2,3} < 0.017$
	Lesion conspicuity	1.50 ± 0.53	2.00 ± 0.76	2.38 ± 0.92	2.38 ± 0.92	0.002, $P_{1,2,3} > 0.017$
	Overall image quality	2.00 ± 0.76	2.50 ± 0.53	3.13 ± 0.83	3.50 ± 0.76	0.001, $P_{2,3} < 0.017$

Note.— Values presented indicate mean ± standard deviation. *P values indicate result of Friedman test, $^{\dagger}P_1$, P_2, and P_3 indicate result of Wilcoxon test: P_1 indicates difference between FBP and AIDR-mild reconstruction mode; P_2 indicates difference between FBP and AIDR-standard reconstruction mode; and P_3 indicates difference between FBP and AIDR-strong mode, respectively. AIDR = adaptive iterative dose reduction, FBP = filtered back projection, Mild = mild reconstruction algorithm, STD = standard reconstruction algorithm, STR = strong reconstruction algorithm, 3D = three-dimensional

with 24 cm, 30 cm, and 40 cm, we obtained the following results (Table 4).

In the 30-cm phantom model, the image noise significantly improved with the AIDR 3D compared to that of the FBP ($p < 0.017$), although the overall image quality was significantly different between the FBP and the AIDR 3D strong reconstruction mode ($p < 0.017$) only. Moreover, the lesion of conspicuity also improved with standard and strong settings of AIDR 3D if compared to FBP ($p < 0.017$). For the 40-cm phantom model, both the image noise and the overall image quality improved with the use of the AIDR 3D standard and strong settings ($p < 0.017$) (Fig. 4). Also, in particular, the image noise, improved with all AIDR 3D algorithms in 40-cm phantom ($p < 0.017$). With regard to the lesion conspicuity, there was significant improvement in the 30-cm phantom with standard and strong AIDR 3D algorithms only. Strong mode had the greatest overall image quality score in the 40-cm phantom ($p < 0.017$) and a similar tendency was shown in the 30-cm phantom ($p < 0.17$). However, in the 24-cm phantom, although the image quality improved with the strength increase of the AIDR 3D algorithm, no significant distinction in image quality resulted ($p > 0.05$) statistically speaking. The impact of AIDR 3D algorithm on noise, lesion conspicuity and image quality were different according to phantom size by qualitative assessment.

DISCUSSION

In our study, AIDR 3D was able to significantly lower the image noise. It enhanced SNR and CNR in variable phantoms without image-quality degradation and achieved better image quality in a large-sized phantom also. According to a previous study (27), the noise index as the parameter indicative of the level of image noise, is proportional to the inverse square root of the dose. Therefore, a reduction of the tube current time product with AIDR 3D is expected compared with FBP while maintaining the same image noise and equivalent image quality. For example, in our study, the stronger AIDR reconstruction method significantly reduced the image noise level in a range of 12–58% if compared to the FBP reconstruction method. In addition, the AIDR 3D strong setting significantly enhanced CNR in a range of 45–114% in all three phantoms also. Our study results are in good agreement with those of previous studies regarding IR algorithms. Also it demonstrates that they not only reduce the radiation dose without image deterioration, but also reduce image noise as well as improving both the SNR and the CNR (20, 28, 29).

Also our study presents with regard to the image quality assessment for AIDR 3D and FBP, that AIDR 3D provided improved image noise if compared with that of FBP reconstruction at the same tube current time product. Furthermore the study demonstrated that AIDR 3D provided at least a similar image quality at the same time-tube current product to FBP, regardless of the strength of the AIDR reconstruction. Also the AIDR 3D strong setting showed better image quality than FBP in the 40-cm phantom. Considering the image quality of FBP technique can be lower in patients with large body habitus if compared with patients with small and intermediate body habitus, due to an increased noise and inadequate image

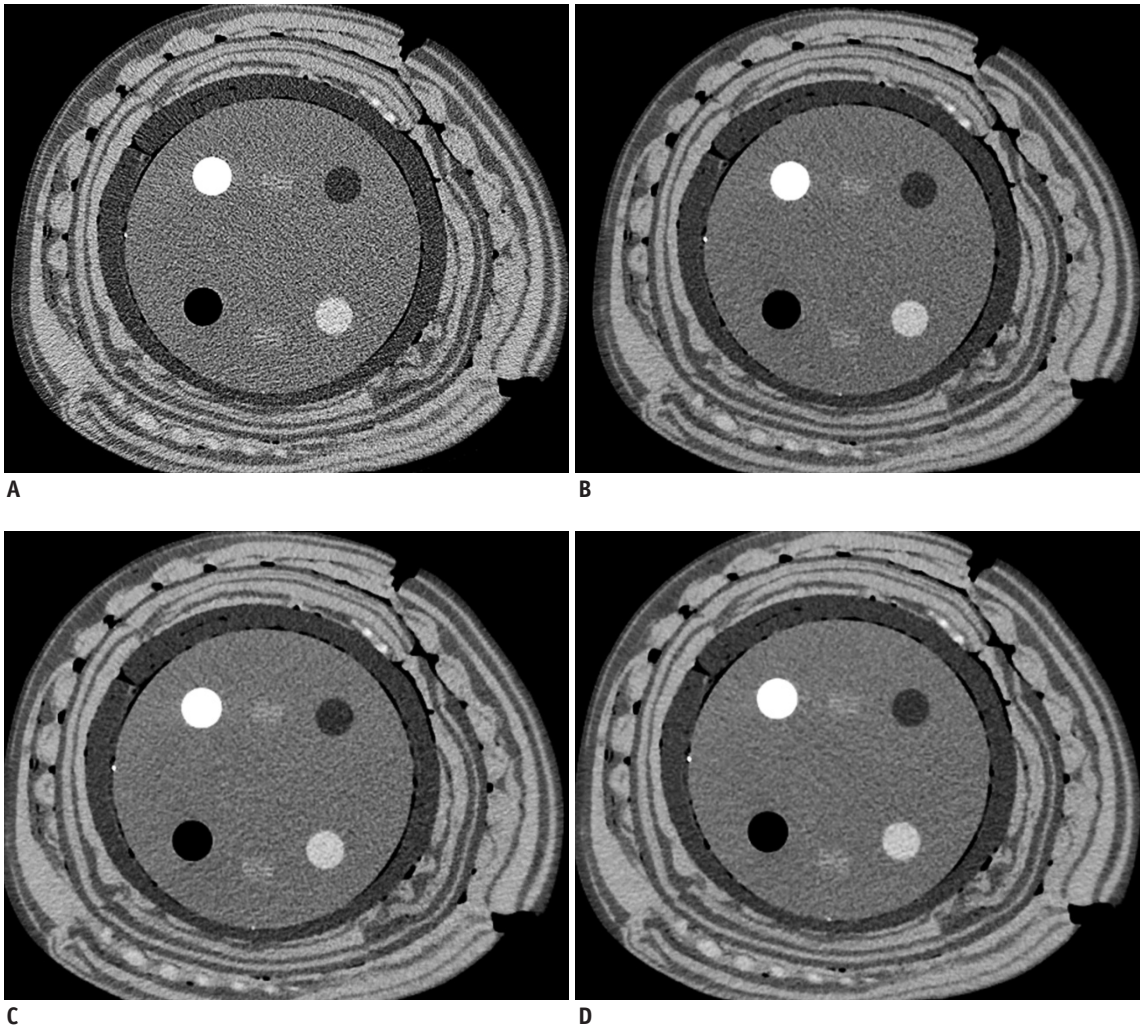

Fig. 4. CT images of 40-cm phantom scanned with tube current time product of 180 mAs reconstructed with filtered back projection (A), adaptive iterative dose reduction three-dimensional mild (B), standard (C), and strong modes (D).

contrast due to underpenetration of X-rays, the superior results of AIDR 3D in the large phantom could be attributed to a significant reduction of noise and an enhancement of contrast within a strong setting (7). Therefore, we may expect within the same noise level, the radiation dose which is required to produce an image should diminish with the use of the AIDR 3D technique. Currently, IR technique modifications are often being installed in numerous types of CT scanners, although their implementation differs for each manufacturer. ASIR (GE Healthcare), iDOSE (Philips Healthcare), and SAFIRE (Siemens Healthcare) techniques require the choice of a percentage of the mixture between FBP and IR images, and the dose reduction as well as the final image quality depend on these parameters (20, 23, 30-33). However, until now, the changes of imaging characteristics with the use of various IR techniques may affect the CT performance for a diagnosis finding as choosing a too large percentage of ASIR or a too high strength of the SAFIRE or iDOSE techniques could result in image over-smoothing or plastic image features caused by the changes in the image noise spectra (16, 34). According to a previous study on AIDR (20), AIDR 3D may be less susceptible to the imaging over-smoothing effect as it automatically chooses the number of iteration. Therefore, if we can reproduce these phantom results in the actual clinical setting, it would be beneficial as we could reduce the radiation dose while maintaining the image quality.

We also evaluated the effectiveness of the AIDR 3D technique according to different patient body sizes using the different-sized phantoms which were specially designed to mimic patients' different body sizes. Regardless of the phantom size, the AIDR 3D technique improved the image quality by reducing image noise as well as improved the SNR and CNR compared with FBP techniques. In addition,

Korean Journal of Radiology
KJR

the percentage of noise reduction of AIDR 3D was greater in the 30-cm phantom than in the 24-cm phantom also: the average percentage of noise reduction of AIDR 3D standard setting compared with FBP in 24-cm, 30-cm, and 40-cm phantoms were 23%, 36%, and 51%, respectively. Furthermore, the effectiveness of the AIDR 3D algorithm on image noise reduction compared with FBP was greater in the 40-cm phantom compared with 24-cm or 30-cm phantoms. Also the effect of image noise reduction by AIDR 3D algorithm compared with FBP technique was confirmed by the reviewers in our qualitative analysis. However, although quantitative results demonstrated that AIDR 3D could enhance SNR and CNR significantly compared with FBP by reducing image noise, an overall image quality improvement by AIDR 3D was achieved only with some algorithm in the 30-cm and 40-cm phantom, mimicking large body habitus patients. Although AIDR 3D provided at least similar or slight better image quality than FBP, it failed to achieve better image quality than FBP in the 24-cm phantoms. We could conclude from these results that the effect of the AIDR 3D algorithm may increase as patients' body size increases, and a stronger IR setting of AIDR 3D could be more beneficial than other settings in patients with large body habitus due to its stronger noise reduction effect.

Our study had several limitations. First, the used phantoms were modifications of the ACR CT accreditation phantom using pork belly fat. As the ACR phantom is designed to be used for CT accreditation programs, the phantom may not effectively represent the actual clinical scenario seen in humans. Second, we analyzed only the acrylic material and the background of the phantom among the 4 modules of the ACR phantom, although module 1 contained several materials such as bone, air, water, polyethylene and acryl. Third, although we used pork-belly fat in order to mimic the different body sizes of human beings, the content of pork-belly fat might differ from that of the human abdominal wall. Fourth, the evaluation on the cons of the IR imaging, such as over-smoothing effect, artificial texture and blotchy appearance, have not been discussed in this study. Therefore, a further study should be performed for a more accurate comparison of AIDR 3D to other imaging methods. Fifth, the diagnostic effectiveness of the AIDR 3D data set was not assessed in comparison with the FBP data set. Instead, we performed an assessment of technical efficacy, in terms of image quality, SNR and CNR for dose reduction only. A further study should be performed on the diagnostic performance of IR algorithms in order to demonstrate its real clinical value in comparison with the conventional FBP algorithm. Last, we did not use the automatic dose-modulation technique with AIDR 3D technique in our study although the AIDR 3D algorithm can be used with the automatic dose-modulation technique (^{SURE}Exposure controls 3D, Toshiba Medical Systems Corporation). When AIDR 3D is used together with the automatic dose-modulation program (^{SURE}Exposure controls 3D, Toshiba Medical Systems Corporation), it may simplify the workflow and theoretically it is less concerned with image smoothing together with radiation-dose reduction (20).

In conclusion, our phantom study shows that compared to traditional FBP images, the AIDR 3D algorithm is effective for reducing the image noise level as well as improving the image-quality parameters, such as the CNR and SNR. The effectiveness of the AIDR 3D algorithm may increase as a phantom size increases. However, further clinical evaluation is required in order to confirm the effectiveness of dose reduction on image-quality preservation when using AIDR 3D.

REFERENCES

1. Brenner DJ, Hall EJ. Computed tomography--an increasing source of radiation exposure. *N Engl J Med* 2007;357:2277-2284
2. Mahesh M. Medical radiation exposure with focus on CT. *Rev Environ Health* 2010;25:69-74
3. Berrington de González A, Mahesh M, Kim KP, Bhargavan M, Lewis R, Mettler F, et al. Projected cancer risks from computed tomographic scans performed in the United States in 2007. *Arch Intern Med* 2009;169:2071-2077
4. Smith-Bindman R, Lipson J, Marcus R, Kim KP, Mahesh M, Gould R, et al. Radiation dose associated with common computed tomography examinations and the associated lifetime attributable risk of cancer. *Arch Intern Med* 2009;169:2078-2086
5. Voress M. The increasing use of CT and its risks. *Radiol Technol* 2007;79:186-190
6. Sagara Y, Hara AK, Pavlicek W, Silva AC, Paden RG, Wu Q. Abdominal CT: comparison of low-dose CT with adaptive statistical iterative reconstruction and routine-dose CT with filtered back projection in 53 patients. *AJR Am J Roentgenol* 2010;195:713-719
7. McCollough CH, Primak AN, Braun N, Kofler J, Yu L, Christner J. Strategies for reducing radiation dose in CT. *Radiol Clin North Am* 2009;47:27-40
8. Marin D, Nelson RC, Rubin GD, Schindera ST. Body CT: technical advances for improving safety. *AJR Am J Roentgenol* 2011;197:33-41

9. McCollough CH, Guimarães L, Fletcher JG. In defense of body CT. *AJR Am J Roentgenol* 2009;193:28-39
10. Halliburton SS, Abbara S, Chen MY, Gentry R, Mahesh M, Raff GL, et al. SCCT guidelines on radiation dose and dose-optimization strategies in cardiovascular CT. *J Cardiovasc Comput Tomogr* 2011;5:198-224
11. Koshy S, Thompson RC. Review of radiation reduction strategies in clinical cardiovascular imaging. *Cardiol Rev* 2012;20:139-144
12. Hara AK, Paden RG, Silva AC, Kujak JL, Lawder HJ, Pavlicek W. Iterative reconstruction technique for reducing body radiation dose at CT: feasibility study. *AJR Am J Roentgenol* 2009;193:764-771
13. Rogalla P, Kloeters C, Hein PA. CT technology overview: 64-slice and beyond. *Radiol Clin North Am* 2009;47:1-11
14. Kalender WA, Buchenau S, Deak P, Kellermeier M, Langner O, van Straten M, et al. Technical approaches to the optimisation of CT. *Phys Med* 2008;24:71-79
15. Yamada Y, Jinzaki M, Tanami Y, Shiomi E, Sugiura H, Abe T, et al. Model-based iterative reconstruction technique for ultralow-dose computed tomography of the lung: a pilot study. *Invest Radiol* 2012;47:482-489
16. Xu J, Mahesh M, Tsui BM. Is iterative reconstruction ready for MDCT? *J Am Coll Radiol* 2009;6:274-276
17. Hwang HJ, Seo JB, Lee JS, Song JW, Kim SS, Lee HJ, et al. Radiation dose reduction of chest CT with iterative reconstruction in image space - Part I: studies on image quality using dual source CT. *Korean J Radiol* 2012;13:711-719
18. Hwang HJ, Seo JB, Lee JS, Song JW, Kim SS, Lee HJ, et al. Radiation dose reduction of chest CT with iterative reconstruction in image space - Part II: assessment of radiologists' preferences using dual source CT. *Korean J Radiol* 2012;13:720-727
19. Goo HW. CT radiation dose optimization and estimation: an update for radiologists. *Korean J Radiol* 2012;13:1-11
20. Gervaise A, Osemont B, Lecocq S, Noel A, Micard E, Felblinger J, et al. CT image quality improvement using Adaptive Iterative Dose Reduction with wide-volume acquisition on 320-detector CT. *Eur Radiol* 2012;22:295-301
21. Utsunomiya D, Weigold WG, Weissman G, Taylor AJ. Effect of hybrid iterative reconstruction technique on quantitative and qualitative image analysis at 256-slice prospective gating cardiac CT. *Eur Radiol* 2012;22:1287-1294
22. Yu L, Bruesewitz MR, Thomas KB, Fletcher JG, Kofler JM, McCollough CH. Optimal tube potential for radiation dose reduction in pediatric CT: principles, clinical implementations, and pitfalls. *Radiographics* 2011;31:835-848
23. Pontana F, Pagniez J, Flohr T, Faivre JB, Duhamel A, Remy J, et al. Chest computed tomography using iterative reconstruction vs filtered back projection (Part 1): evaluation of image noise reduction in 32 patients. *Eur Radiol* 2011;21:627-635
24. Gupta AK, Nelson RC, Johnson GA, Paulson EK, Delong DM, Yoshizumi TT. Optimization of eight-element multi-detector row helical CT technology for evaluation of the abdomen. *Radiology* 2003;227:739-745
25. Desai GS, Uppot RN, Yu EW, Kambadakone AR, Sahani DV. Impact of iterative reconstruction on image quality and radiation dose in multidetector CT of large body size adults. *Eur Radiol* 2012;22:1631-1640
26. Kalra MK, Maher MM, Blake MA, Lucey BC, Karau K, Toth TL, et al. Detection and characterization of lesions on low-radiation-dose abdominal CT images postprocessed with noise reduction filters. *Radiology* 2004;232:791-797
27. Kanal KM, Stewart BK, Kolokythas O, Shuman WP. Impact of operator-selected image noise index and reconstruction slice thickness on patient radiation dose in 64-MDCT. *AJR Am J Roentgenol* 2007;189:219-225
28. Tatsugami F, Matsuki M, Nakai G, Inada Y, Kanazawa S, Takeda Y, et al. The effect of adaptive iterative dose reduction on image quality in 320-detector row CT coronary angiography. *Br J Radiol* 2012;85:e378-e382
29. Martinsen AC, Sæther HK, Hol PK, Olsen DR, Skaane P. Iterative reconstruction reduces abdominal CT dose. *Eur J Radiol* 2012;81:1483-1487
30. Prakash P, Kalra MK, Ackman JB, Digumarthy SR, Hsieh J, Do S, et al. Diffuse lung disease: CT of the chest with adaptive statistical iterative reconstruction technique. *Radiology* 2010;256:261-269
31. Silva AC, Lawder HJ, Hara A, Kujak J, Pavlicek W. Innovations in CT dose reduction strategy: application of the adaptive statistical iterative reconstruction algorithm. *AJR Am J Roentgenol* 2010;194:191-199
32. Pontana F, Duhamel A, Pagniez J, Flohr T, Faivre JB, Hachulla AL, et al. Chest computed tomography using iterative reconstruction vs filtered back projection (Part 2): image quality of low-dose CT examinations in 80 patients. *Eur Radiol* 2011;21:636-643
33. Mitsumori LM, Shuman WP, Busey JM, Kolokythas O, Koprowicz KM. Adaptive statistical iterative reconstruction versus filtered back projection in the same patient: 64 channel liver CT image quality and patient radiation dose. *Eur Radiol* 2012;22:138-143
34. Thibault JB, Sauer KD, Bouman CA, Hsieh J. A three-dimensional statistical approach to improved image quality for multislice helical CT. *Med Phys* 2007;34:4526-4544